PAPER

Check for updates

Effect of cation alkyl chain length on 3-sulfopropylmethacrylate-based draw solutes having lower critical solution temperature

Jihyeon Moon and Hyo Kang [ID] *

We investigated the effect of change in alkyl chain length of cation in tributylalkylphosphonium 3-sulfopropyl methacrylate ([P$_{444\#}$][C$_3$S], # = 4, 6, and 8) ionic liquids (ILs) on their osmolality and recovery properties as the draw solute in the forward osmosis (FO) process. The ILs aqueous solutions exhibited a characteristic of the lower critical solution temperature (LCST)-type phase separation, which allowed for the easy recovery of the draw solute or clean water from the diluted draw solution. The LCSTs of 31, 26, 22, and 18 °C were obtained from 2.5, 5.0, 7.5, and 10.0 wt% aqueous solutions of [P$_{4446}$][C$_3$S]. When deionized water, 2000 ppm NaCl solution, and 10.0 wt% orange juice aqueous solution were used as feed solution, the water fluxes of the aqueous [P$_{4446}$][C$_3$S] solutions were approximately 4.49, 3.87, and 1.55 LMH, respectively, in the active layer facing the draw solution mode at 7.5 wt% of draw solution. This study demonstrates the applicability of a thermoresponsive ionic structure material as a draw solute for the FO process.

Introduction

The demand for freshwater is increasing owing to the growing population and economy, and environmental deterioration worldwide.[1–3] Membrane-based separation technologies including reverse osmosis (RO), have been used for wastewater treatment to provide high-quality water for industrial as well as domestic purposes. However, these technologies consume a large amount of energy,[4] facilitating the need for energy-efficient water and wastewater treatments. Forward osmosis (FO) is a membrane separation technology that drives the transportation of water molecules from the diluted solution side to the concentrated solution side by the chemical gradient potential rather than hydraulic pressure. This natural phenomenon demonstrates that the osmosis system of the FO process does not require external energy, enabling energy-efficient water treatment.[5,6] The FO process also has other advantages such as reduced membrane fouling potential, strong adaptability to other treatment technologies, and easy membrane cleaning.[7–9] Owing to these reasons, the FO process is often applied for water reuse, power production, liquid food concentration, pharmaceutical concentration, and fertilizer.[10–14] Despite plenty of strength of the FO process, several challenges remain. The final product of the FO process, using a draw solution as an osmotic agent, is a diluted draw solution. Therefore, recovering the draw solute or pure water from the

diluted draw solution is an essential step in the FO process after the water is transferred to the draw solution side of the membrane. This recovery process is an energy-intensive step in FO.[15] To achieve an efficient FO process, both the water-drawing ability and easy regeneration of the draw solute must be considered.[16,17]

Several researchers have proposed various draw solutes that meet these criteria. Draw solutes can be categorized as nonresponsive or responsive. The water affinity of responsive draw solutes undergoes reversible changes upon responding to external stimuli, such as electric and magnetic fields, gas, salt, pH, light, and temperature.[18–35] Table 1 presents the previous research on responsive draw solutes. The responsiveness of responsive draw solutes enables the facile separation of the draw solute after the water permeation process, making them more attractive than non-responsive draw solutes. Among the responsive draw solutes, thermoresponsive draw solutes with temperature-dependent solubility are more favorable compared with other responsive draw solutes in the regeneration process. Because their phase transition in water can be driven by a mild temperature change using an inexpensive heat source including waste or geothermal heat during draw solute regeneration.[36,37] Thermoresponsive draw solutes undergo two types of temperature-dependence phase transition between homogeneous phase and separated liquid/liquid bi-phase. The increase of miscibility of the draw solute with water upon heating above the critical temperature (T_c) is a characteristic of the upper critical solution temperature (UCST)-type draw solute. In contrast, the lower critical solution temperature (LCST)-type

BK-21 Four Graduate Program, Department of Chemical Engineering, Dong-A University, 37 Nakdong-Daero 550 Beon-gil, Saha-gu, Busan 49315, Republic of Korea. E-mail: hkang@dau.ac.kr; Fax: +82 51 200 7728; Tel: +82 51 200 7720

Table 1 Summary of the responsive draw solutes for the FO process

Stimulation factor	Draw solution	Osmotic pressure/draw solution concentration	Feed solution	Water flux (L m^{-2} h^{-1})	Ref.
Electric field	AMPS/DMAEMA	—^{a}/—	2000 ppm NaCl	2.09	19
	HA–PVA-5	—/—	2000 ppm NaCl	1.34	20
Magnetic field	D-Bu-FeX$_4$	3500 mOsm kg^{-1}/25 wt%	3.5 wt% NaCl	4.50	21
	Gelatin-MNP	1.48 atm/27 g L^{-1}	Deionized (DI) water	1.54	22
Gas	PDMAEMA	1208 mOsm kg^{-1}/0.3 g g^{-1}	DI water	6.3	23
	SPS-DMCHA	—/5 mol kg^{-1}	0.5 mol kg^{-1} NaCl	11.0	24
	Ammonia-CO$_2$	193.3 atm/4.5 M	0.5 M NaCl	20.8	25
	P(DEAEMA-PEGDA)	—/0.1 g, 50% water	2000 ppm NaCl	56.0	26
Salt	MgSO$_4$	—/240 000 ppm	5050 ppm NaCl	4.1	27
pH	(NH$_4$)$_6$Mo$_7$O$_{24}$	/0.4 M	DI water	10.0	28
Light	PSA-NIPAM-C	—/—	2000 ppm NaCl	0.77	29
Temperature	[Hbet][Tf$_2$N]	—/3.20 M	DI water	2.27	30
	[N$_{2222}$]Br	—/0.50 M	DI water	10.65	31
	[N$_{4444}$]2,4,6-MeBnSO$_3$	58.2 atm/2 M	DI water	12.31	32
	HM8I	—/60 wt%	0.60 M NaCl	4.60	33
	GE$_7$B$_3$	28 atm/56 wt%	Milli-Q water	4.81	34
	BuMP	28.6 atm/55 wt%	DI water	2.09	35
	[P$_{4446}$][C$_3$S]	258 mOsm kg^{-1}/7.5 wt%	DI water	4.49	This work
			2000 ppm NaCl	3.87	

^{a} Unidentified values in each reference.

draw solute in a homogeneous phase state becomes immiscible upon cooling below the T_c.

Various types of thermoresponsive draw solutions had been explored, among them, ionic liquids (ILs) have attracted much attention. ILs, which are organic salts that have a melting point of less than 100 °C can dissociate in water-forming ions, leading to osmolality.[38,39] ILs also have attractive characteristics including negligible volatility, high ion density and ionic conductivity, tunable polarity, basicity, and acidity.[40–43] The most crucial feature of ILs is the ability of their physicochemical properties to be tuned by modification of their alkyl chain length and an ionic precursor according to application requirements, such as electrochemistry,[44] catalysis,[45,46] and extraction.[47] As to LCST-type ILs, there are many cation–anion combinations composed of tetrabutylphosphonium cations ([P$_{4444}$]$^+$) and different anions, especially sulfonate type and amino acid type anions.[48,49] The LCST-type phase behavior and miscibility of ILs in water were dependent strongly on the total hydrophobicity of ions composed ILs as reported by Kohno *et al.*[50] The hydrophobicity of ions can be tuned by the varying alkyl chain length of the component ions and comparison between ion species with different hydrophobicity. Therefore, understanding the structure–property relationship of the thermoresponsive IL molecular structure and its properties can provide a deeper insight into future developments in draw solutes with a better balance between the drawing ability and recovery properties. Among various ILs, we have explored the applicability of the ILs composed of tributylalkylphosphonium cation and 3-sulfopropylmethacrylate anion. According to previous reports, phosphonium-based ILs have shown high thermal and chemical stability.[51–53] The 3-sulfopropylmethacrylate anions show the possibility to have a good balance of osmotic and recovery properties when combined with

phosphonium cation. In addition, 3-sulfopropylmethacrylate is low in cost and easily available for practical application.

Therefore, this study investigates the correlations between the molecular structure of ILs and its drawing ability and recovery properties to design efficient draw solutes by increasing the length of the alkyl chain of tributylalkylphosphonium ([P$_{4444}$], [P$_{4446}$], and [P$_{4448}$]) in LCST-type 3-sulfopropylmethacrylate-based ILs. The effect of change in the alkyl chain length of cation in ILs on their FO performance and LCST-type phase behavior has been systematically observed. Our investigations provide a strong reference for the design and synthesis of thermoresponsive ionic materials as prospective draw solutions.

Experimental

Materials

Tetrabutylphosphonium bromide (99%) ([P$_{4444}$]Br), tributyl(hexyl)phosphonium bromide (98%) ([P$_{4446}$]Br), tributyl(octyl)phosphonium bromide (98%) ([P$_{4448}$]Br), and 3-sulfopropyl methacrylate potassium salt (>97%) (K[C$_3$S]) were purchased from Tokyo Chemical Industry Co., Ltd. Dichloromethane was purchased from Daejung Chemicals and Metals Co., Ltd.

Preparation of ILs, tributylalkylphosphonium 3-sulfopropyl methacrylate ([P$_{444\#}$][C$_3$S])

ILs, tributylalkylphosphonium 3-sulfopropyl methacrylate ([P$_{444\#}$][C$_3$S], where # is the alkyl chain length in tributylalkylphosphonium) were prepared *via* anion exchange. [P$_{444\#}$]Br (15 mmol), and K[C$_3$S] (40 mmol) were dissolved in deionized (DI) water and were stirred for 18 h at 25 ± 1 °C. After the reaction time, products were extracted by dichloromethane and

rinsed with DI water. Dichloromethane was evaporated by a rotary evaporator and dried *in vacuo* at 30 °C to obtain the ILs. $[P_{4444}][C_3S]$, $[P_{4446}][C_3S]$, and $[P_{4448}][C_3S]$ were obtained in a single step with 74, 70, and 71% yield, respectively. $[P_{444\#}][C_3S]$ structure and composition were analyzed by proton nuclear magnetic resonance (^1H NMR) spectroscopy. To confirm the physical properties of the ILs, the densities (ρ) and melting temperatures (T_m) of the ILs were analyzed. It is observed that ILs have densities with values ranging from 1.08 to 1.14 g mL^{-1} at 25 ± 1 °C. In addition, the melting temperatures of the ILs were observed in the temperature range of 6 to 17 °C.

$[P_{4444}][C_3S]$. ^1H NMR (400 MHz, CDCl$_3$, δ/ppm): $\delta = 0.76$–0.92 (t, 12H, CH_3–CH$_2$–CH$_2$–), 1.32–1.50 (m, 16H, –CH$_2$–CH$_2$–CH$_2$–P$^+$–), 1.75–1.84 (t, 3H, CH_3–C$_2$H$_2$–CO$_2$–), 2.03–2.30 (m, 10H, SO$_3$$^-$–CH$_2$–$CH_2$–, CH$_2$–$CH_2$–P$^+$), 2.70–2.83 (m, 2H, SO$_3$$^-$–CH$_2$–CH$_2$–), 4.06–4.19 (t, 2H, –CH$_2$–CH_2–O–), 5.36–5.44, 5.91–5.99 (d, 2H, $CH_2 = C_2H_3$–CO$_2$–), ρ: 1.14 g mL^{-1}, T_m: 12 °C.

$[P_{4446}][C_3S]$. ^1H NMR (400 MHz, CDCl$_3$, δ/ppm): $\delta = 0.80$–1.03 (t, 12H, CH_3–CH$_2$–CH$_2$–), 1.21–1.36 (m, 4H, CH$_3$–CH_2–CH$_2$–CH$_2$–CH$_2$–CH$_2$–P$^+$–), 1.41–1.60 (m, 16H, –CH$_2$–CH$_2$–CH$_2$–P$^+$–), 1.83–1.94 (t, 3H, CH_3–C$_2$H$_2$–CO$_2$–), 2.13–2.42 (m, 10H, SO$_3$$^-$–CH$_2$–$CH_2$–, CH$_2$–$CH_2$–P$^+$), 2.82–2.96 (m, 2H, SO$_3$$^-$–$CH_2$–CH$_2$–), 4.17–4.30 (t, 2H, –CH$_2$–CH_2–O–), 5.43–5.51, 6.00–6.08 (d, 2H, $CH_2 = C_2H_3$–CO$_2$–), ρ: 1.09 g mL^{-1}, T_m: 6 °C.

$[P_{4448}][C_3S]$. ^1H NMR (400 MHz, CDCl$_3$, δ/ppm): $\delta = 0.75$–1.01 (t, 12H, CH_3–CH$_2$–CH$_2$–), 1.12–1.33 (m, 8H, CH$_3$–CH_2–CH$_2$–CH$_2$–CH$_2$–CH$_2$–), 1.37–1.59 (m, 16H, –CH$_2$–CH$_2$–CH$_2$–P$^+$–), 1.82–1.91 (t, 3H, CH_3–C$_2$H$_2$–CO$_2$–), 2.07–2.44 (m, 10H, SO$_3$$^-$–CH$_2$–$CH_2$–, CH$_2$–$CH_2$–P$^+$), 2.78–2.93 (m, 2H, SO$_3$$^-$–$CH_2$–CH$_2$–), 4.12–4.31 (t, 2H, –CH$_2$–CH_2–O–), 5.43–5.50, 5.98–6.09 (d, 2H, $CH_2 = C_2H_3$–CO$_2$–), ρ: 1.08 g mL^{-1}, T_m: 17 °C.

Forward osmosis performance

Water and reverse solute fluxes were measured with a U-shaped FO system by connecting two custom-made L-shaped glass tubes. A thin-film composite membrane (Hydration Technologies Inc.) was placed in a channel with a diameter of 2.1 cm in the FO system. The prepared IL aqueous solution was added as the draw solution and DI water was added as the feed solution. Water and reverse solute fluxes were measured in the different modes, the active layer facing the draw solution (AL-DS) and the active layer facing the feed solution (AL-FS) mode at a temperature of 22 ± 1 °C. Both solutions were stirred by a magnetic bar. The water flux (J_w, L m^{-2} h^{-1}, LMH) is the rate of the permeating water and can be quantified by eqn (1).

$$J_w = \frac{\Delta V}{A \Delta t} \tag{1}$$

where ΔV represents the permeate volume of the feed solution across the membrane, Δt is the operating time, and A is an effective membrane area of 3.32×10^{-4} m^2.

The reverse solute flux (J_s, g m^{-2} h^{-1}, gMH) indicates the quantity of the draw solute transport through the membrane to the feed side and was calculated from the total dissolved solids (TDS) in the feed solution. The reverse solute flux was measured from the conductivity value difference of the feed solution before and after FO, as described in eqn (2).

$$J_s = \frac{\Delta(CV)}{A \Delta t} \tag{2}$$

where ΔC represents the concentration change, ΔV is the permeate volume of the feed solution.

Instruments

The structure analyses of the prepared ILs were performed by ^1H NMR spectroscopy (MR400 DD2 NMR, Agilent Technologies, Inc.) and Fourier transform infrared (FT-IR) spectroscopy (Nicolet iS20, Thermo Fisher Scientific). The density of the IL was determined by calculating the ratio of its mass to its volume four or more times. To analyze the melting temperatures of the prepared ILs which are liquid at 25 ± 1 °C, a Q-10 (TA Instruments, Inc.) equipped with RCS40 (TA Instruments, Inc) was employed by differential scanning calorimetry (DSC) under a nitrogen atmosphere at the cooling rate and heating rate of 1 °C min^{-1} in the temperature range from -90 to 50 °C. The viscosity of the ILs was measured at 85 s^{-1} shear rate using a DV-III programmable rheometer (Brookfield) with rotating a metallic spindle. The conductivities of the IL aqueous solutions were measured using a conductivity meter (Seven2CO pro, METTLER TOLEDO). The osmolalities of the IL aqueous solutions were determined using an osmometer (SEMI-MICRO OSMOMETER K-7400, KNAUER). The phase transition temperatures of the IL aqueous solutions were determined using an ultraviolet-visible (UV-vis) spectrophotometer (EMC-11D-V, EMCLAB Instruments GmbH) and a temperature controller (TC200P, Misung Scientific Co., Ltd).

Results and discussion

Preparation and characterization of ILs, tributylalkylphosphonium 3-sulfopropyl methacrylate ($[P_{444\#}][C_3S]$)
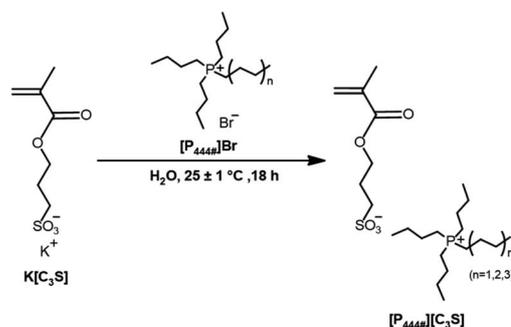
Fig. 1 shows the preparative scheme for the tributylalkylphosphonium 3-sulfopropyl methacrylate ($[P_{444\#}][C_3S]$, where # is the alkyl chain length in tributylalkylphosphonium), *via* an anion exchange reaction of $[P_{4444}]$Br, $[P_{4446}]$Br, and $[P_{4448}]$Br with K$[C_3S]$. The structures of $[P_{444\#}][C_3S]$ were determined by ^1H NMR and FT-IR analysis in attenuated total reflection mode

Fig. 1 Preparative scheme for tributylalkylphosphonium 3-sulfopropyl methacrylate ($[P_{444\#}][C_3S]$, where # is the alkyl chain length in tributylalkylphosphonium).

before the FO experiments. The ^{1}H NMR spectra of the ILs tetrabutylphosphonium 3-sulfopropyl methacrylate ([P_{4444}][C_3S]), (b) tributyl(hexyl)phosphonium 3-sulfopropyl methacrylate ([P_{4446}][C_3S]), and (c) tributyl(octyl)phosphonium 3-sulfopropyl methacrylate ([P_{4448}][C_3S]) were illustrated in Fig. 2(a)–(c). The ^{1}H NMR spectrum (Fig. 2(a)) of [P_{4444}][C_3S] indicates the presence of a vinyl group of 3-sulfopropyl methacrylate (δ/ppm = δ = 5.36–5.44 (peak b) and δ = 5.91–5.99 (peak c)) and the methyl proton of 3-sulfopropyl methacrylate (δ/ppm = δ = 1.75–1.84 (peak a), δ = 4.06–4.19 (peak d), δ = 2.03–2.30 (peak e), and δ = 2.70–2.83 (peak f)). The presence of alkyl groups of the tetrabutylphosphonium was also confirmed (δ/ppm = δ = 2.03–2.30 (peak g), δ = 1.32–1.50 (peak h), and δ = 0.76–0.92 ppm (peak i)). The degree of anion exchange of [P_{4444}][C_3S] can be interpreted by comparing the ratio of the integral area of the respective proton peaks of the alkyl groups. Similarly, the successful synthesis of [P_{4446}][C_3S] and [P_{4448}][C_3S] were observed (Fig. 2(b) and (c)). Furthermore, the FT-IR spectra allow for the comparison of the chemical structures of [P_{4444}][C_3S], [P_{4446}][C_3S], and [P_{4448}][C_3S] with those of [P_{4444}]Br, [P_{4446}]Br, [P_{4448}]Br, and K[C_3S], as shown in Fig. 3. The peaks corresponding to the C–H bond appeared at 2933 and 2868 cm^{-1}. The peak of the C=O bond in the 3-sulfopropyl methacrylate is detected at 1713 cm^{-1}. The peaks are observed at 1179 and 1035 cm^{-1} corresponding to the S=O bond in the 3-sulfopropyl methacrylate, respectively. This result suggests that the anion of [P_{4444}]Br was successfully exchanged with 3-sulfopropyl methacrylate (Fig. 3). The solubility and thermoresponsive behavior of ILs can be tuned by modification of their structure.[54,55] To confirm the phase behaviors of the ILs, we mixed the ILs, [P_{4444}][C_3S], [P_{4446}][C_3S], and [P_{4448}][C_3S] with DI water as a function of the concentrations (weight percent, wt%) of the ILs in water. [P_{4444}][C_3S] and [P_{4446}][C_3S] with a concentration from 2.5 to 10.0 wt% dissolved in water at 18 ± 1 °C to form homogeneous phases. When the concentration exceeds 10.0 wt%, heterogeneous distribution of [P_{4446}][C_3S] in water is observed at 18 ± 1 °C. In contrast, [P_{4448}][C_3S] was barely soluble in the same condition which means that measurements of its solution properties were impossible. The affinity of IL with water is governed by its hydrophobicity. In particular, an increase in the hydrophobic
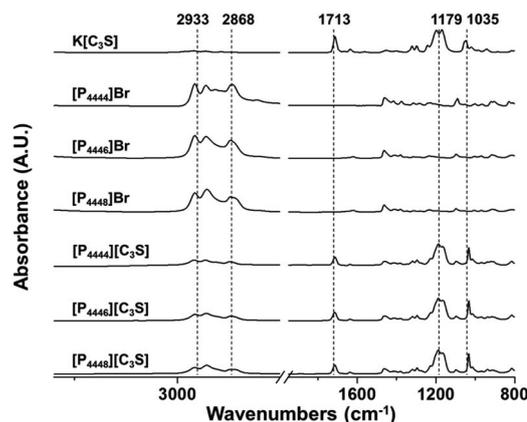
Fig. 3 FT-IR spectra of K[C_3S], [$P_{444\#}$]Br, and [$P_{444\#}$][C_3S].

alkyl chain length leads to a decrease in the affinity of IL with water.[49,50,56] Therefore, the IL-bearing excessively hydrophobic cation is insoluble in water.

Viscosity

The viscosity of the draw solution influences the water drawing property of the draw solution in the FO process. The low viscosity of the draw solution leads to high water fluxes. Because a high viscosity of the draw solution causes an unfavorable effect on the water flow across the membrane, leading to severe internal polarization concentration (ICP).[57] Therefore, the viscosities of the [P_{4444}][C_3S] and [P_{4446}][C_3S] aqueous solutions with good solubility in water were measured at a temperature of 18 ± 1 °C by varying the concentration from 2.5 to 10.0 wt% of the IL concentration. Fig. 4a and b show the viscosities of the [P_{4444}][C_3S] and [P_{4446}][C_3S] aqueous solutions, respectively. The viscosities of the [P_{4444}][C_3S] aqueous solutions are 0.24, 0.66, 0.72, and 1.6 cP at concentrations of 2.5, 5.0, 7.5, and 10.0 wt%, respectively. The viscosities of the [P_{4446}][C_3S] aqueous solutions are 0.96, 1.27, 1.33, and 2.80 cP at the same concentrations. As shown in Fig. 4, the viscosities of [P_{4444}][C_3S] and [P_{4446}][C_3S] aqueous solutions were increased with increasing
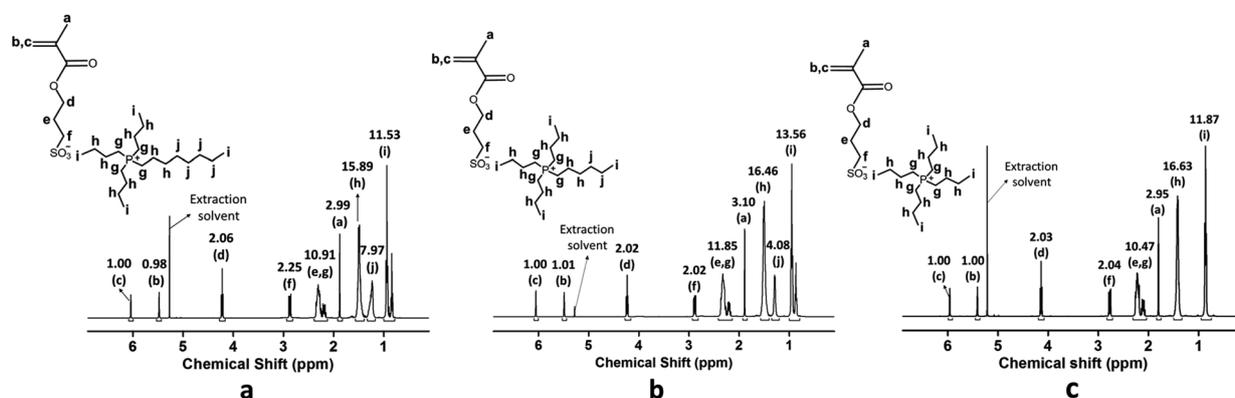
Fig. 2 ^{1}H NMR spectra: (a) tetrabutylphosphonium 3-sulfopropyl methacrylate ([P_{4444}][C_3S]), (b) tributyl(hexyl)phosphonium 3-sulfopropyl methacrylate ([P_{4446}][C_3S]), and (c) tributyl(octyl)phosphonium 3-sulfopropyl methacrylate ([P_{4448}][C_3S]).
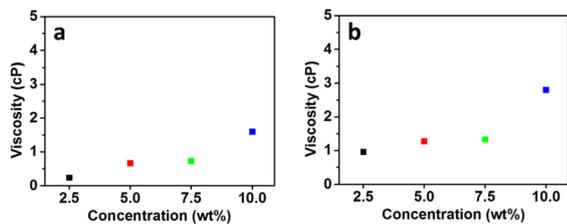
Fig. 4 Viscosities of (a) $[P_{4444}][C_3S]$ and (b) $[P_{4446}][C_3S]$ aqueous solutions according to solution concentration.

concentration. Furthermore, it was observed that $[P_{4446}][C_3S]$ has relatively higher viscosities than $[P_{4444}][C_3S]$ at all concentrations. Because the van der Waals interaction leads to ion aggregation with the elongation of the alkyl chain.[58]

Conductivity

Ionic conductivity which depends on the degree of ionic dissociation in ILs aqueous solutions relates to the charge carrier concentrations and ion mobility of ILs.[59,60] In addition, the conductivity of ILs is associated with their osmolality.[61] The change in the chain length of the cation influences the conductivity of the IL; thus, the conductivities of the $[P_{4444}][C_3S]$ and $[P_{4446}][C_3S]$ aqueous solutions with good solubility in water were measured at different concentrations. Fig. 5 shows that the conductivities of the $[P_{4444}][C_3S]$ and $[P_{4446}][C_3S]$ aqueous solutions increase with increasing concentrations of the draw solutions from 2.5 to 10.0 wt%. Ions present in the solution transport charge, indicate that conductivity increases with increasing ion concentration.[60,62–65] The conductivities of $[P_{4444}][C_3S]$ aqueous solutions were approximately 1914, 3161, 4157, and 5022 $\mu S\ cm^{-1}$ at concentrations of 2.5, 5.0, 7.5, and 10.0 wt%, respectively. The conductivities of the $[P_{4446}][C_3S]$ aqueous solutions were approximately 1630, 2675, 3442, and 3734 $\mu S\ cm^{-1}$ at the same concentrations. The conductivities of the ILs decrease at all concentrations as the alkyl chain length of the quaternary phosphonium in the IL increases from 4 to 6 CH_2 units in $[P_{444\#}][C_3S]$ ILs. Typically, ILs with large ion sizes lead to a decrease in ionic conductivity. The cation size increases along with the alkyl chain elongation of the cation, leading to a reduction in the charge carriers and ion mobility. Because the alkyl chain elongation leads to the enhancement of their van der Waals interaction, resulting in ion aggregation.[66–68] Therefore, $[P_{4444}][C_3S]$ containing $[P_{4444}]^+$ ions with short alkyl
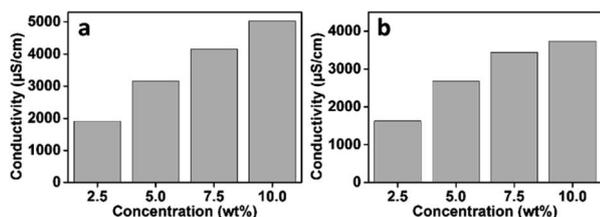
chain length show a relatively high conductivity compared to $[P_{4446}][C_3S]$.

Osmotic pressure

The high osmotic pressure of the draw solution in comparison to the feed solution enhances the water permeability in the FO system because the permeation of the water across a membrane is driven by the osmotic pressure gradient.[36,69]

As the osmotic pressure is a colligative property, the osmotic pressure of the draw solute is proportional to its concentration.[70] The osmotic pressures of $[P_{4444}][C_3S]$ and $[P_{4446}][C_3S]$ aqueous solutions were measured at different concentrations of ILs to investigate their usability as draw solutes, as can be seen in Fig. 6. The osmotic pressures of the $[P_{4444}][C_3S]$ aqueous solutions were approximately 131, 189, 302, and 428 mOsmol kg^{-1} at concentrations of 2.5, 5.0, 7.5, and 10.0 wt%, respectively. However, the osmotic pressures of the $[P_{4446}][C_3S]$ aqueous solutions were lower than that of $[P_{4444}][C_3S]$. The values were approximately 81, 137, 258, and 365 mOsmol kg^{-1} at the same concentrations. Increasing the concentrations of $[P_{4444}][C_3S]$ and $[P_{4446}][C_3S]$ in water caused an increase in the osmotic pressure. Furthermore, the osmotic pressure of the IL decreases at all concentrations along with the alkyl chain elongation of the quaternary phosphonium in the IL, $[P_{444\#}][C_3S]$, owing to their amphiphilic properties. As aforementioned the osmotic pressure is governed by the number of solutes, the greater the degree of ionization of ILs in water, the higher the osmotic pressure of ILs.[71,72] The ionization ability of ILs depends on the hydrophobic alkyl chain length; ILs with longer alkyl chain lengths are likely to lead to weaker solvation of the ILs with water and stronger aggregation of the ILs.[73–76] Therefore, $[P_{4444}][C_3S]$, which has more hydrophilic cations due to the alkyl chains being shorter than hexyl, displays a higher osmotic pressure in water than the $[P_{4446}][C_3S]$ aqueous solutions at all concentrations.

Recovery property

In the FO process, the separation of pure water and draw solutes from the draw solution is necessary for their recovery.[77] To improve the energy efficiency of recovery, thermoresponsive ILs were synthesized and used as draw solutes in this study. The LCST, one of the thermoresponsive properties, is the phase separation temperature at which the LCST-type ILs aqueous
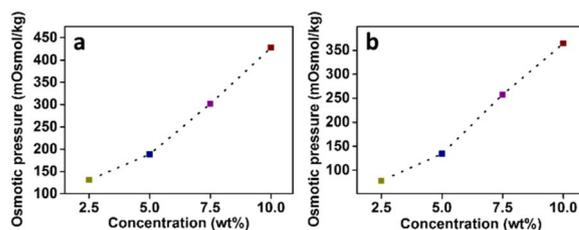

Fig. 5 Conductivities of (a) $[P_{4444}][C_3S]$ and (b) $[P_{4446}][C_3S]$ aqueous solutions according to solution concentration.

Fig. 6 Osmotic pressures of (a) $[P_{4444}][C_3S]$ and (b) $[P_{4446}][C_3S]$ aqueous solutions according to solutions concentration measured by freezing point depression method.

solutions become milky at a temperature above the LCST. We examined the phase behavior of the prepared ILs in water using their thermoresponsive properties to investigate the possibility of using the draw solute. $[P_{4448}][C_3S]$ was barely soluble in water at room temperature, and no phase transitions were observed. In contrast, $[P_{4444}][C_3S]$ and $[P_{4446}][C_3S]$ dissolved homogeneously under the same conditions, and the $[P_{4446}][C_3S]$ aqueous solution exhibited an LCST-type phase transition. The LCST of the $[P_{4446}][C_3S]$ aqueous solution was determined by observing the transmittance curve based on the temperature change using a UV-vis spectrophotometer at 550 nm with a temperature controller. The transmittance *versus* temperature curves of the $[P_{4446}][C_3S]$ aqueous solutions marked changes at each Tc for concentrations of 2.5, 5.0, 7.5, and 10.0 wt%, as shown in Fig. 7. We define the LCST as the temperature corresponding to 50% transmittance. As the concentration of the $[P_{4446}][C_3S]$ aqueous solution increased, the LCST decreased. At each concentration, the LCST transitions of the $[P_{4446}][C_3S]$ aqueous solutions were approximately 31, 26, 22, and 18 °C, respectively. The LCST behavior of an aqueous solution typically has the following equation, where ΔG_{mix}, ΔH_{mix}, and ΔS_{mix} are the free energy, enthalpy, and entropy of mixing, respectively.[78–80]

$$\Delta G_{mix} = \Delta H_{mix} - T\Delta S_{mix} \qquad (3)$$

When the ΔG_{mix} changes from negative to positive, the LCST-type phase separation occurs. The interactive forces between water and anions or cations and those between anions and cations play a key role in the LCST behavior of IL in an aqueous solution.[50] In the IL aqueous solution system, at $T <$ LCST, the IL and water mixture formed a homogeneous state leading to a negative ΔH_{mix}, whereas at $T >$ LCST, the phase separation of the IL and water is driven by a negative ΔS_{mix}. Therefore, in our system, the interaction force between $[P_{4446}]^+$ and $[C_3S]^-$ is strong compared to that between $[P_{4446}][C_3S]$ and water molecules at the temperature above its LCST and causes phase separation of the $[P_{4446}][C_3S]$.

Water and reverse solute fluxes

The water and reverse solute fluxes of the $[P_{4446}][C_3S]$ as the draw solute were measured in AL-DS and AL-FS modes using a custom-made FO system, because only $[P_{4446}][C_3S]$ has
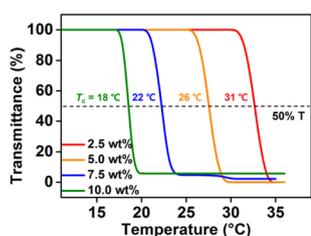
a thermo-responsive property that allows easy regeneration of the draw solute. A semipermeable FO membrane was placed between two connecting custom-made glass tubes. One side was filled with DI water as the feed solution, whereas the other side was filled with $[P_{4446}][C_3S]$ aqueous solution as the draw solution at concentrations of 2.5, 5.0, and 7.5 wt%. The measurements were performed at a temperature below its LCST. Since low temperature causes low water flux, the water flux of the $[P_{4446}][C_3S]$ aqueous solution with an LCST of 18 °C at 10.0 wt% concentration was not measured. The osmotically driven water flux was determined by measuring the difference in the height of the solution before and after the FO. The water flux increased with increasing concentration of $[P_{4446}][C_3S]$ aqueous solutions in both the AL-DS and AL-FS modes, as shown in Fig. 8. The water fluxes of the $[P_{4446}][C_3S]$ aqueous solutions were 2.53, 3.04, and 4.49 LMH in AL-DS mode at concentrations of 2.5, 5.0, and 7.5 wt%, respectively, and 1.45, 2.90, and 3.98 LMH in AL-FS mode, respectively, for the same concentrations. A linear relationship between water flux and concentration was observed, as expected from the osmotic pressure results. These results indicate that sufficient osmotic pressure drives the water permeation process in FO. The reverse solute flux which is denoted as the cross-diffusion of permeating solute to the feed solution side was calculated from the final and initial TDS concentration of the feed solution.[81] The reverse solute fluxes of the $[P_{4446}][C_3S]$ aqueous solutions were 1.65, 2.54, and 1.64 gMH in the AL-DS mode at concentrations of 2.5, 5.0, and 7.5 wt%, respectively, and 0.87, 1.59, and 1.03 gMH in AL-FS mode, respectively, for the same concentrations. At each concentration, in AL-DS mode, the water fluxes of the $[P_{4446}][C_3S]$ aqueous solutions were higher compared with those in AL-FS mode. The main reason is related to the ICP.[82] The dilutive ICP is a phenomenon that causes dilution of the draw solution due to the water permeating within the membrane support layer. A significant dilutive ICP which takes place in AL-FS mode leads
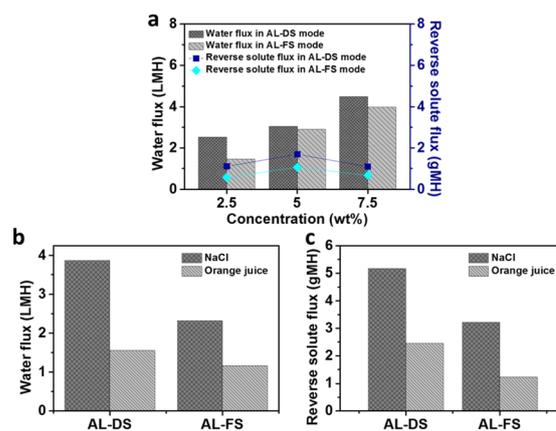

Fig. 8 (a) Water fluxes and reverse solute fluxes results using $[P_{4446}][C_3S]$ aqueous solutions as draw solution according to the concentration and DI water as feed solution in AL-DS and AL-FS modes, (b) water fluxes, and (c) reverse solute fluxes results using 7.5 wt% $[P_{4446}][C_3S]$ aqueous solution as draw solution and 2000 ppm NaCl solution and 10.0 wt% orange juice aqueous solution as feed solution in AL-DS and AL-FS modes at a temperature of 22 ± 1 °C.

Fig. 7 Transmittance curves of $[P_{4446}][C_3S]$ aqueous solutions according to solutions concentration measured by the temperature change using UV-vis spectrophotometer.

to a decrease in the osmotic pressure gradient, resulting in water flux reduction.[83,84] To investigate the applicability of the $[P_{4446}][C_3S]$ as the draw solute, the water and reverse solute fluxes of the FO process using 7.5 wt% $[P_{4446}][C_3S]$ aqueous solution as draw solution were measured while 2000 ppm NaCl solution and 10.0 wt% orange juice aqueous solution were used as feed solution. Fig. 8 shows the water and reverse solute fluxes in the different modes, AL-DS and AL-FS modes at a temperature of 22 ± 1 °C. When 2000 ppm NaCl solution was a feed solution, the water fluxes were 3.87 and 2.32 LMH in the AL-DS and AL-FS modes, respectively. The reverse solute fluxes were 5.17 and 3.22 gMH in the AL-DS and AL-FS modes, respectively. In addition, when using 10.0 wt% orange juice aqueous solution as feed solution, the water fluxes were 1.55 and 1.16 LMH in the AL-DS and AL-FS modes, respectively. The reverse solute fluxes were 2.45 and 1.22 gMH in the AL-DS and AL-FS modes, respectively. These results show potential applications of the thermoresponsive ILs as the draw solute for brackish water desalination and food processing.

Conclusions

We prepared tributylalkylphosphonium 3-sulfopropyl methacrylate ($[P_{444\#}][C_3S]$, where # is the alkyl chain length in tributylalkylphosphonium) to investigate its utility in the FO process. In aqueous solutions, $[P_{4446}][C_3S]$ showed LCSTs in the range of 2.5 to 10.0 wt%, which enables its easy regeneration at the recovery step in the FO system. The LCSTs of $[P_{4446}][C_3S]$ were approximately 31, 26, 22, and 18 °C at concentrations of 2.5, 5.0, 7.5, and 10.0 wt%, respectively. When DI water was a feed solution, the water flux and reverse solute flux of $[P_{4446}][C_3S]$ aqueous solution of 7.5 wt% were 4.49 LMH and 1.64 gMH in AL-DS mode, and 3.89 LMH and 1.03 gMH in AL-FS mode at 22 ± 1 °C. Furthermore, when 2000 ppm NaCl solution and 10.0 wt% orange juice aqueous solution were used as feed solution, the water fluxes were 3.87 and 1.55 LMH in AL-Ds mode, respectively. This study provides an important approach for the design of thermoresponsive organic materials as draw solutes owing to their reasonable FO performance and energy-efficient recovery.

Author contributions

Jihyeon Moon: investigation, validation, formal analysis, data curation, writing-original draft, writing-review & editing, visualization; Hyo Kang: conceptualization, methodology, validation, resources, writing-original draft, writing-review & editing, supervision, project administration, funding acquisition.

Conflicts of interest

There are no conflicts to declare.

Acknowledgements

References

1 F. Dolan, J. Lamontagne, R. Link, M. Hejazi, P. Reed and J. Edmonds, *Nat. Commun.*, 2021, **12**, 1–10.

2 M. M. Mekonnen and A. Y. Hoekstra, *Sci. Adv.*, 2016, **2**, e1500323.

3 M. Elimelech and W. A. Phillip, *Science*, 2011, **333**, 712–717.

4 A. Haupt and A. Lerch, *Membranes*, 2018, **8**, 47.

5 T. Y. Cath, A. E. Childress and M. Elimelech, *J. Membr. Sci.*, 2006, **281**, 70–87.

6 W. Suwaileh, N. Pathak, H. Shon and N. Hilal, *Desalination*, 2020, **485**, 114455.

7 S. E. Kwan, E. Bar-Zeev and M. Elimelech, *J. Membr. Sci.*, 2015, **493**, 703–708.

8 M. Xie, J. Lee, L. D. Nghiem and M. Elimelech, *J. Membr. Sci.*, 2015, **493**, 748–754.

9 Y. Kim, M. Elimelech, H. K. Shon and S. Hong, *J. Membr. Sci.*, 2014, **460**, 206–212.

10 X. Zhou, D. B. Gingerich and M. S. Mauter, *Ind. Eng. Chem. Res.*, 2015, **54**, 6378–6389.

11 R. L. McGinnis and M. Elimelech, *Environ. Sci. Technol.*, 2008, **42**, 8625–8629.

12 L. A. Handojo, K. Khoiruddin, A. K. Wardani, A. N. Hakim and I. G. Wenten, *IOP Conf. Ser.: Mater. Sci. Eng.*, 2019, **547**, 012053.

13 K. W. Hameed, *Iraqi J. Chem. Pet. Eng.*, 2013, **14**, 71–79.

14 Y. Cui and T. Chung, *Nat. Commun.*, 2018, **9**, 1–9.

15 D. J. Johnson, W. A. Suwaileh, A. W. Mohammed and N. Hilal, *Desalination*, 2018, **434**, 100–120.

16 T. Takahashi, K. Akiya, T. Niizeki, M. Matsumoto and T. Hoshina, *Colloids Surf., A*, 2022, **639**, 128372.

17 T. Chung, X. Li, R. C. Ong, Q. Ge, H. Wang and G. Han, *Curr. Opin. Chem. Eng.*, 2012, **1**, 246–257.

18 Y. Cai, *Desalination*, 2016, **391**, 16–29.

19 H. Cui, H. Zhang, M. Yu and F. Yang, *Desalination*, 2018, **426**, 118–126.

20 H. Zhang, J. Li, H. Cui, H. Li and F. Yang, *Chem. Eng. J.*, 2015, **259**, 814–819.

21 Q. Zhao and D. L. Zhao, *Chem. Eng. J. Adv.*, 2023, **14**, 100446.

22 F. Azadi, A. Karimi-Jashni and M. M. Zerafat, *Environ. Technol.*, 2021, **42**, 2885–2895.

23 Y. Cai, W. Shen, R. Wang, W. B. Krantz, A. G. Fane and X. Hu, *Chem. Comm.*, 2013, **49**, 8377–8379.

24 C. J. Orme and A. D. Wilson, *Desalination*, 2015, **371**, 126–133.

25 J. R. McCutcheon, R. L. McGinnis and M. Elimelech, *J. Membr. Sci.*, 2006, **278**, 114–123.

26 H. Rabiee, B. Jin, S. Yun and S. Dai, *Chem. Eng. J.*, 2018, **347**, 424–431.

27 R. Alnaizy, A. Aidan and M. Qasim, *Desalin. Water Treat.*, 2013, **51**, 5516–5525.

28 Y. Shi, X. Liao, R. Chen and Q. Ge, *Environ. Sci. Technol.*, 2021, **55**, 12664–12671.

29 D. Li, X. Zhang, J. Yao, Y. Zeng, G. P. Simon and H. Wang, *Soft Matter*, 2011, **7**, 10048–10056.

30 Y. Zhong, X. Feng, W. Chen, X. Wang, K. Huang, Y. Gnanou and Z. Lai, *Environ. Sci. Technol.*, 2016, **50**, 1039–1045.

31 H. G. Zeweldi, L. A. Limjuco, A. P. Bendoy, H. Kim, M. J. Park, H. K. Shon, E. M. Johnson, H. Lee, W. Chung and G. M. Nisola, *Desalination*, 2018, **444**, 94–106.

32 H. G. Zeweldi, A. P. Bendoy, M. J. Park, H. K. Shon, H. Kim, E. M. Johnson, H. Kim, S. Lee, W. Chung and G. M. Nisola, *Desalination*, 2020, **495**, 114635.

33 J. Park, H. Joo, M. Noh, Y. Namkoong, S. Lee, K. H. Jung, H. R. Ahn, S. Kim, J. Lee and J. H. Yoon, *J. Mater. Chem. A*, 2018, **6**, 1255–1265.

34 A. Inada, K. Yumiya, T. Takahashi, K. Kumagai, Y. Hashizume and H. Matsuyama, *J. Membr. Sci.*, 2019, **574**, 147–153.

35 A. Inada, T. Takahashi, K. Kumagai and H. Matsuyama, *Ind. Eng. Chem. Res.*, 2019, **58**, 12253–12260.

36 Y. Cai, W. Shen, J. Wei, T. H. Chong, R. Wang, W. B. Krantz, A. G. Fane and X. Hu, *Environ. Sci.: Water Res. Technol.*, 2015, **1**, 341–347.

37 D. Nakayama, Y. Mok, M. Noh, J. Park, S. Kang and Y. Lee, *Phys. Chem. Chem. Phys.*, 2014, **16**, 5319–5325.

38 T. Endo, K. Sunada, H. Sumida and Y. Kimura, *Chem. Sci.*, 2022, **13**, 7560–7565.

39 A. Kokorin, in *Ionic liquids: theory, properties, new approaches*, BoD–Books on Demand GmbH, Norderstedt, 2011.

40 J. S. Wilkes and M. J. Zaworotko, *J. Chem. Soc., Chem. Commun.*, 1992, **13**, 965–967.

41 T. Welton, *Chem. Rev.*, 1999, **99**, 2071–2084.

42 N. V. Plechkova and K. R. Seddon, *Chem. Soc. Rev.*, 2008, **37**, 123–150.

43 P. Wasserscheid and T. Welton, in *Ionic liquids in synthesis*, Wiley Online Library, Hoboken, 2008.

44 A. Abo-Hamad, M. A. AlSaadi, M. Hayyan, I. Juneidi and M. A. Hashim, *Electrochim. Acta*, 2016, **193**, 321–343.

45 J. P. Hallett and T. Welton, *Chem. Rev.*, 2011, **111**, 3508–3576.

46 Z. Duan, Y. Gu, J. Zhang, L. Zhu and Y. Deng, *J. Mol. Catal. A: Chem.*, 2006, **250**, 163–168.

47 B. Tang, W. Bi, M. Tian and K. H. Row, *J. Chromatogr. B: Anal. Technol. Biomed. Life Sci.*, 2012, **904**, 1–21.

48 J. Cui, Y. Li, D. Chen, T. Zhan and K. Zhang, *Adv. Funct. Mater.*, 2020, **30**, 2005522.

49 Y. Kohno and H. Ohno, *Chem. Commun.*, 2012, **48**, 7119–7130.

50 Y. Kohno and H. Ohno, *Phys. Chem. Chem. Phys.*, 2012, **14**, 5063–5070.

51 C. Maton, N. De Vos and C. V. Stevens, *Chem. Soc. Rev.*, 2013, **42**, 5963–5977.

52 C. J. Bradaric, A. Downard, C. Kennedy, A. J. Robertson and Y. Zhou, *Green Chem.*, 2003, **5**, 143–152.

53 M. Stalpaert, F. G. Cirujano and D. E. De Vos, *ACS Catal.*, 2017, **7**, 5802–5809.

54 M. Smiglak, J. M. Pringle, X. Lu, L. Han, S. Zhang, H. Gao, D. R. Macfarlane and R. D. Rogers, *Chem. Commun.*, 2014, **50**, 9228–9250.

55 S. Dong, J. Heyda, J. Yuan and C. A. Schalley, *Chem. Commun.*, 2016, **52**, 7970–7973.

56 K. A. Kurnia, C. M. Neves, M. G. Freire, L. M. Santos and J. A. Coutinho, *J. Mol. Liq.*, 2015, **210**, 264–271.

57 D. Zhao, S. Chen, P. Wang, Q. Zhao and X. Lu, *Ind. Eng. Chem. Res.*, 2014, **53**, 16170–16175.

58 L. Sun, O. Morales-Collazo, H. Xia and J. F. Brennecke, *J. Phys. Chem. B*, 2016, **120**, 5767–5776.

59 H. Xu, D. Zhao, P. Xu, F. Liu and G. Gao, *J. Chem. Eng. Data*, 2005, **50**, 133–135.

60 H. Every, A. G. Bishop, M. Forsyth and D. R. Macfarlane, *Electrochim. Acta*, 2000, **45**, 1279–1284.

61 R. B. Campbell, C. A. Bower and L. A. Richards, *Soil Sci. Soc. Am. J.*, 1949, **13**, 66–69.

62 M. Sha, H. Dong, F. Luo, Z. Tang, G. Zhu and G. Wu, *J. Phys. Chem. Lett.*, 2015, **6**, 3713–3720.

63 J. M. Otero-Mato, H. Montes-Campos, V. Gómez-González, M. Montoto, O. Cabeza, S. Kondrat and L. M. Varela, *J. Mol. Liq.*, 2022, **355**, 118955.

64 V. V. Chaban, I. V. Voroshylova, O. N. Kalugin and O. V. Prezhdo, *J. Phys. Chem. B*, 2012, **116**, 7719–7727.

65 E. Rilo, J. Vila, S. García-Garabal, L. M. Varela and O. Cabeza, *J. Phys. Chem. B*, 2013, **117**, 1411–1418.

66 N. R. Pitawela and S. K. Shaw, *ACS Meas. Sci. Au*, 2021, **1**, 117–130.

67 W. Yuan, X. Yang, L. He, Y. Xue, S. Qin and G. Tao, *Front. Chem.*, 2018, **6**, 59.

68 G. Adamová, R. L. Gardas, L. P. N. Rebelo, A. J. Robertson and K. R. Seddon, *Dalton Trans.*, 2011, **40**, 12750–12764.

69 J. R. McCutcheon, R. L. McGinnis and M. Elimelech, *Desalination*, 2005, **174**, 1–11.

70 J. van't Hoff, *Proc. Phys. Soc., London*, 1887, **9**, 307.

71 M. Silberberg-Bouhnik, O. Ramon, I. Ladyzhinski, S. Mizrahi and Y. Cohen, *J. Polym. Sci., Part B: Polym. Phys.*, 1995, **33**, 2269–2279.

72 S. J. Bates, *J. Am. Chem. Soc.*, 1915, **37**, 1421–1445.

73 R. F. Rodrigues, A. A. Freitas, J. N. Canongia Lopes and K. Shimizu, *Molecules*, 2021, **26**, 7159.

74 D. C. Belchior, T. E. Sintra, P. J. Carvalho, M. R. Soromenho, J. M. Esperança, S. P. Ventura, R. D. Rogers, J. A. Coutinho and M. G. Freire, *J. Chem. Phys.*, 2018, **148**, 193842.

75 K. Kawai, K. Kaneko and T. Yonezawa, *Langmuir*, 2011, **27**, 7353–7356.

76 H. Wang, J. Wang, S. Zhang, Y. Pei and K. Zhuo, *ChemPhysChem*, 2009, **10**, 2516–2523.

77 D. Li, X. Zhang, G. P. Simon and H. Wang, *Water Res.*, 2013, **47**, 209–215.

78 C. Zhao, Z. Ma and X. X. Zhu, *Prog. Polym. Sci.*, 2019, **90**, 269–291.

79 G. Pasparakis and C. Tsitsilianis, *Polymer*, 2020, **211**, 123146.

80 H. Kang, D. E. Suich, J. F. Davies, A. D. Wilson, J. J. Urban and R. Kostecki, *Commun. Chem.*, 2019, **2**, 51.

81 M. Ferby, S. Zou and Z. He, *Environ. Sci.: Water Res. Technol.*, 2020, **6**, 423–435.

82 G. T. Gray, J. R. McCutcheon and M. Elimelech, *Desalination*, 2006, **197**, 1–8.

83 J. R. McCutcheon and M. Elimelech, *AIChE J.*, 2007, **53**, 1736–1744.

84 J. R. McCutcheon and M. Elimelech, *J. Membr. Sci.*, 2006, **284**, 237–247.